The 32nd International Workshop on Water Waves and Floating Bodies, Dalian, China, 23-26 April, 2017.

The kinematics in a plunging breaker revisited.

Y.-M. Scolan
ENSTA-Bretagne (France), yves-marie.scolan@ensta-bretagne.fr

Highlights

- Fully nonlinear free surface problems, Potential theory,
- Fluid kinematics and shape of a plunging breaker, Location of maximum velocity.

1) Introduction

The kinematics in the fluid of a plunging breaker has been abundantly studied in the past. The pioneering works by John (1953) for the theoretical developments and by Miller (1957) for the experimental observations are often cited in the papers that appeared in 70s and early 80s. Among those papers, the contributions by Longuet-Higgins (1980, 1981, 1982 and later papers) are significant. In particular the initiation of the overturning crest or the tracking of the free surface with very small radius of curvature (quasi sharp corners) can be handled analytically with a Lagrangian approach in the absence of gravity. The plunging breaker is also modelled by fitting a tear-drop shaped domain to the inner fluid boundaries of the barrel (also known as the tube by surfers). New (1983) shows that the aspect ratio of an ellipse that partly fits the barrel boundary, is almost time-invariant. Based on the same idea, Jenkins (1994) provides stationary solutions (in potential theory) of the plunging jet. However those solutions are non-physical in the sense that the plunging jet may intersect the foot of the wave and this marks the end of any potential flow modelling.

Numerically the approach proposed by Longuet-Higgins and Cokelet (1976) or Vinje and Brevig (1980) provides the first results for periodic waves. Greenhow (1983), New *et al.* (1985), Dommermuth *et al.* (1988), yield quantitative results concerning the kinematics in the overturning crest. In Peregrine *et al.* (1980), are identified the areas where velocity and acceleration are above or below given thresholds. The region where velocity exceeds the phase velocity is around the crest, while the highest accelerations are in the barrel. The comparisons made by Skyner (1996) show a reasonable overall agreement between numerical (potential flow) and experimental results in terms of kinematics inside the breaker. However, the largest discrepancies occur in the barrel where the radius of curvature is smallest. The experiments performed by Perlin *et al.* (1996) confirm the order of magnitude of the maximum velocity and their analysis of the velocity field also confirms the irrotationality of the flow as long as the free surface does not intersect itself. Yasuda *et al.* (1997) report a numerical comparison of the kinematics in different types of breakers. The time evolution of the regions of highest velocity and acceleration is investigated. They observe that the horizontal velocity is mainly located at the crest of the plunging breaker, whereas the vertical velocity component reaches its highest value in the barrel.

Since then few experimental or numerical analyses have been done on those topics. Even if more and more numerical studies are performed with CFD, the main results obtained with potential theory have not progressed significantly.

Nevertheless recent theoretical work by Constantin (2015) gives a mathematical proof of the existence of the maximum velocity in the barrel. In that paper the location of that maximum is not precisely defined; it is between the crest and the point where the slope along the free surface is infinite. It is the purpose of the present work to give more insights into that theoretical result.

2) Analysis of the velocity in the barrel

Computations with unsteady potential theory are made with the code described in Scolan (2010). The fully nonlinear free surface boundary conditions are satisfied without capillarity. In order to simulate a plunging breaker for different water depths, the numerical code starts with the fluid at rest, with an initial free surface deformation. The flow is described in a coordinate system whose origin is at the left bottom of the tank. The coordinate system (x, y) is oriented as in figures (**??**). These figures show the successive free surface profiles as the overturning crest develops. The initial free surface position is emphasized. The main differences between shallow and deep water breaking are the slope of the free surface on the left side of the barrel, either flat or stiff respectively. In order to set the notations and the terminology, figures (1) show the free surface profile at a given instant before the tip of the jet hits the foot of the wave in shallow water (up) and in deep water (bottom). We can distinguish four geometric points on the free surface where the tangent is either horizontal (points 2 and 3) or vertical (points 1 and

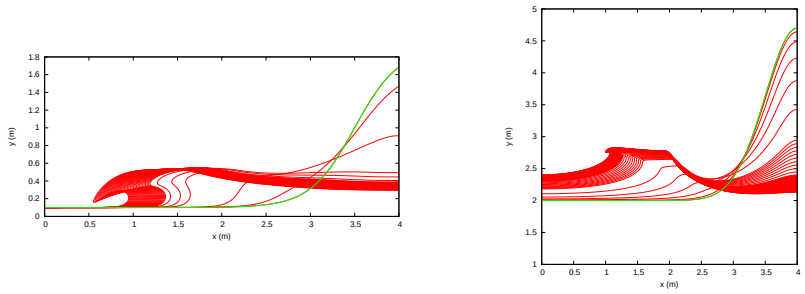

Figure 1: Successive free surface profile. Left: shallow water depth. Right: deep water depth.

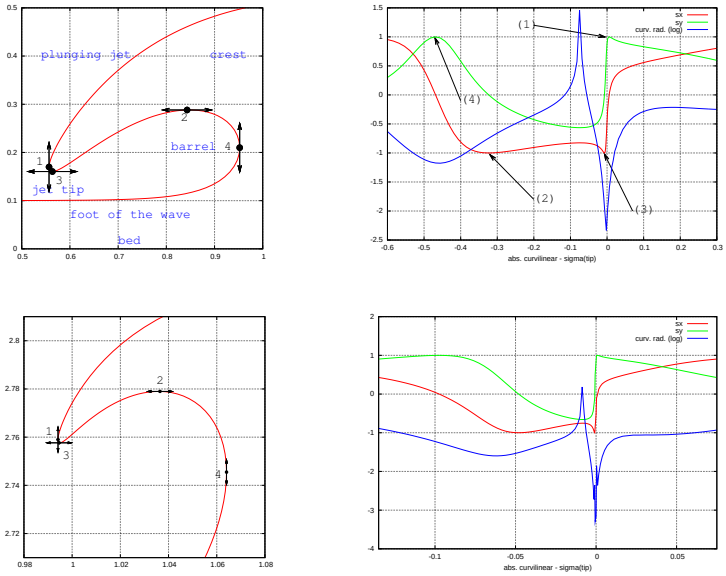

Figure 2: Left: Closer view of the crest. Right: variation with the arclength of the cartesian coordinates (s_x, s_y) of the tangent vector $\vec{s}$ and the $\log_{10}$ of the radius of curvature. Up: shallow water depth. Bottom: deep water depth.

4). The left figures (1) show the variation of the cartesian coordinates of the tangent vector $\vec{s} = (s_x, s_y)$ along the free surface. The arclength along the free surface (also called here curvilinear abscissa) increases from point 4 to point 1 and it is measured positively from left to right. In figures (1), the origin is at the jet tip. The position of the tip is chosen where the velocity of the fluid particle at the free surface is parallel to the normal direction $\vec{n}$. In other words when the normal velocity is maximum and the tangential velocity vanishes and changes sign. It is also the point where the radius of curvature (its $\log_{10}$ is plotted in figures 1 right) is the smallest. The analysis of the velocity distribution yields the location of the maximum horizontal velocity. We plot in figure (2) the temporal variations of two characteristic arclengths: 1) the position of point 2 where $s_y = 0$, and 2) the position of maximum horizontal velocity. It is clear that whatever the considered water depth (shallow: left, deep: right), those two locations on the free surface are very close to each other for all times after the barrel has formed, (after the point 2 appears).

Some properties of the velocity fields follow from the analysis of Euler's equations. Conservation of momentum links the Lagrangian acceleration of a fluid particle to the pressure gradient and gravity as follows

$$\frac{d\vec{u}}{dt} = -\frac{1}{\rho}\vec{\nabla}p + \vec{g}. \tag{1}$$

The table below summarizes the values of the horizontal and vertical accelerations at the four characteristics points ranged as the arclength s inscreases from point #4 to point #1

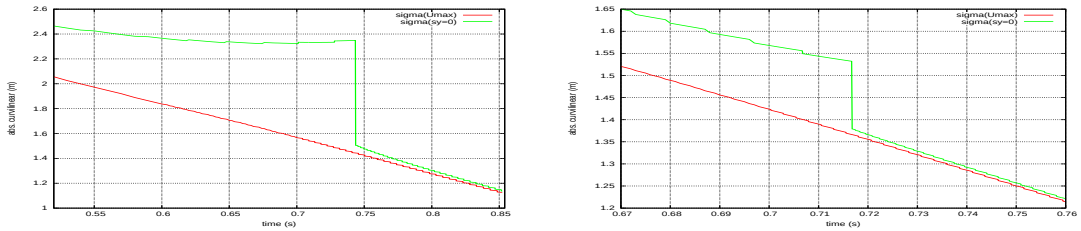

Figure 3: Time variation of the arclength corresponding to the maximum horizontal velocity (red line) and the point 2 (green line).

point #	4	2	3	1
$\frac{d\vec{u}}{dt} \cdot \vec{s}$	$-g$	0	0	$-g$
$\frac{d\vec{u}}{dt} \cdot \vec{n}$	$-p_{,n}/\rho$	$-p_{,n}/\rho + g$	$-p_{,n}/\rho + g$	$-p_{,n}/\rho$
$\frac{dU}{dt}$	$p_{,n}/\rho$	0	0	$p_{,n}/\rho$
$\frac{dV}{dt}$	$-g$	$p_{,n}/\rho - g$	$p_{,n}/\rho - g$	$-g$

We use the theoretical result that $p_{,n}$ is always negative at the free surface (see Constantin, 2011). As a consequence, the modulus of the Lagrangian acceleration is always greater at point 3 than at point 1 as long as the normal gradient of the pressure does not vary much between the two points 1 and 3. We can certainly prove that $|p_{,n}|$ almost vanishes at the crest since the fluid at the tip is in free fall (accelerated by the gravity only). The fluid hence decelerates more along the forward face of the crest than along the barrel. As a consequence, since the horizontal velocities at points 1 and 3 are quite similar, it is expected that $|U_1| < |U_3|$. It should be noted that in the present configuration depicted in the figures (**??**), $U < 0$ all over the fluid in the crest.

Between the points 3 and 2, where the horizontal acceleration is necessarily small since nil at the points 3 and 2, we also expect a slight variation of the horizontal component of the velocity. Since the variation along the arc length s is such that $|U|$ goes on increasing as we approach the point 2, and given that the horizontal velocity $|U|$ decreases dramatically at point 4, the maximum necessarily occurs in the vicinity of point 2. That is precisely observed with the next results.

More surprisingly, it is remarkable that the components of the velocity in the local coordinate system $(\vec{s}, \vec{n})$, respectively denoted $\phi_{,s}$ and $\phi_{,n}$ by using the velocity potential ϕ, have the same variations as s_x and s_y. For the shallow water case, the following approximations can be formulated

$$\phi_{,s} \approx \frac{U_2}{2}(s_x - 1), \qquad \phi_{,n} \approx -U_4 s_y \tag{2}$$

where U_2 and U_4 are the horizontal velocities at points 2 and 4 respectively. At the instant $t = 0.849s$, $U_2 \approx -4.88m/s$ and $U_4 \approx -2.83m/s$. At that instant, figure (3) compares the computed tangential and normal velocities and their approximations from equations (2). The agreement is fairly good along most

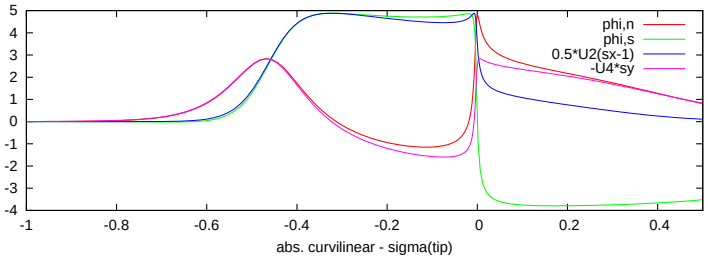

Figure 4: Variation with the arclength of the normal velocity $\phi_{,n}$ and tangential velocity $\phi_{,s}$ at the free surface at time $t = 0.849s$. Superimposition of their approximations in terms of s_x and s_y (see equation 2)

of the barrel $s < 0$. However, those approximations barely reproduce the kinematics in a close vicinity of the crest. The spatial-temporal variations of $\phi_{,s}$ and $\phi_{,n}$ and their approximations are plotted in figure

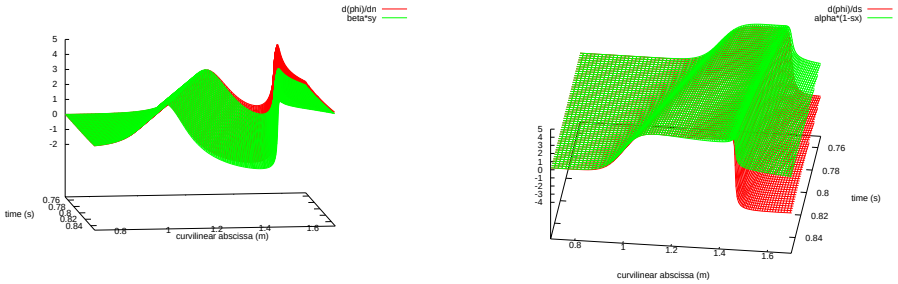

Figure 5: Spatial and temporal variation of the normal velocity $\phi_{,n}$ and tangential velocity $\phi_{,s}$ at the free surface. Superimposition of their approximations in terms of s_x and s_y (see equation 2).

(4). Over time, the validity of those approximations are reasonable as long as U_2 and U_4 do not vary much over time. It should be noted that this result is clearly valid for shallow depth. Its extension to deep water is more questionable. However, at that stage it is remarkable to conclude that the size of the plunging breaker determines the fluid kinematics. This conclusion was also formulated in the past by some authors cited in the introduction.

3) References

• Miller, R. L., 1957, Role of vortices in surf zone prediction: sedimentation and wave forces. *In Beach and Nearshore Sedimentation (ed. R. A. Davis & R. I. Ethington), pp. 92-1 14. SOCE. con. Paleontologists and Mineralogists Spec. Publ. 24.*

• Longuet-Higgins M. S. & Cokelet E. D. 1976, The deformation of steep surface waves on water. I. A numerical method of computation. *Proc. R. Soc. Lond. A* **350**, 1-26.

• Longuet-Higgins M. S., 1980, A Technique for Time-Dependent Free-Surface Flows *Proceedings of the Royal Society of London. Series A*, **371**, 441-451.

• Longuet-Higgins M. S., 1980, On the forming of sharp corners at a free surface, *Proc. R. Soc. Lond. A*, **371**, 453-478.

• Longuet-Higgins M. S., 1981, On the overturning of gravity waves, *Proc. R. Soc. Lond. A*, **376**, 377-400.

• Longuet-Higgins M. S., 1982, Parametric solutions for breaking waves, *Journal of Fluid Mechanics* **121**, 403-424.

• New, A. L. 1983, A class of elliptical free-surface flows. *Journal of Fluid Mechanics* **130**, 219-239.

• Jenkins, A. D., 1994, A stationary potential-flow approximation for a breaking-wave crest *Journal of Fluid Mechanics*, **280**, 335-347.

• New, A.L., McIver P,. & Peregrine D. H. 1985, Computations of overturning waves. *Journal of Fluid Mechanics* **150**, 233-251

• Greenhow M., 1983, Free-surface flows related to breaking waves. *Journal of Fluid Mechanics* **134**, 259-275.

• Dommermuth D. G., Yue D. K. P., Lin W. M., Rapp R. J., Chan E. S. and Melville W. K., 1988, Deep-water plunging breakers: a comparison between potential theory and experiments. *Journal of Fluid Mechanics*, **189**, 423-442.

• Skyner D.., 1996, A comparison of numerical predictions and experimental measurements of the internal kinematics of a deep-water plunging wave. *Journal of Fluid Mechanics*, **315**, 51-64.

• Perlin M., J.-H. He, and L. P. Bernal, 1996, An experimental study of deep water plunging breakers, *Phys. Fluids*, **8** (9), 2365-2374.

• Yasuda T., Mutsuda H., Mizutani N. 1997, Kinematics of overturning solitary waves and their relations to breaker types *Coastal Engineering*, **29**, Issues 3-4, 317-346.

• Constantin A., 2015, The time evolution of the maximal horizontal surface fluid velocity for an irrotational wave approaching breaking. *Journal of Fluid Mechanics*, **768**, 468-475.

• Scolan, Y.-M., 2010, Some aspects of the flip-through phenomenon: A numerical study based on the desingularized technique *J. Fluid Struc.*, **26**, Issue 6, 918-953.

• Constantin A., 2011, Nonlinear Water Waves with Applications to Wave-Current Interactions and Tsunamis, CBMS-NSF Reg. Conf. Ser. Appl. Maths, vol. 81. SIAM.